COMPUTATIONAL MODELS FOR MICRO CHANNEL PLATE SIMULATIONS*

V. Ivanov, Muons, Inc. 522 N. Batavia Ave., Batavia, IL 60510, U.S.A#.

Abstract

Many measurements in particle and accelerator physics are limited by the time resolution with which individual particles can be detected. This includes particle identification via time-of-flight in major experiments like CDF at Fermilab and Atlas and CMS at the LHC, as well as the measurement of longitudinal variables in accelerator physics experiments. Large-scale systems, such as neutrino detectors, could be significantly improved by inexpensive, large-area photo-detectors with resolutions of a few millimetres in space and a few picoseconds in time. The invention of a new method of making micro-channel plates (MCP) promises to yield better resolution and be considerably less expensive than current techniques.

INTRODUCTION

One of the first full numerical models for MCP simulations was suggested by A.J. Guest [1]. Further improvements of this model were done by Y. Kulikov [2] in simulation of spatial resolution for light amplifiers of static images. Here, two different numerical models for short-pulse MCP simulations are suggested [3]. The semi-analytical approach is a powerful tool for the design of static image amplifiers (night vision devices, electron optical converters, streak cameras etc.). Monte Carlo simulations can be successfully used for large area photo detectors with micron and pico-second resolution range. Both approaches have been implemented in the computer codes MCPS [4] and MCS (Monte Carlo Simulator). The results of computer modelling for electric fields and MCP parameters are presented.

ELECTRIC FIELD DISTRIBUTION FOR TILTED CYLINDRICAL CHANNELS IN A DIELECTRIC MEDIUM

The chevron pair is a typical MCP configuration which can prevent ion feedback and increase the efficiency of the first strike problem. It consists of two glass plates with tilted cylindrical pores with a different orientation for each plate. The side surfaces of the plates are metalized, and the voltage V applied to them. The internal surfaces of the pores are coated with a resistive layer and secondary emitter material. Typical dimensions are: plate thickness – 0.5 mm, pore diameter 5-10 um, coatings – 10 nm, tilt angle - 8˚. The field distribution in the pore has a complex structure comparised with straight channels, where the electric field vector is parallel to the z-axis, and the field is a 1D one. This tilted field can change the gain factor of secondary emission in the pore. One can show that the field for the most internal part of the pore can be described analytically, but the fringe fields should be evaluated numerically.

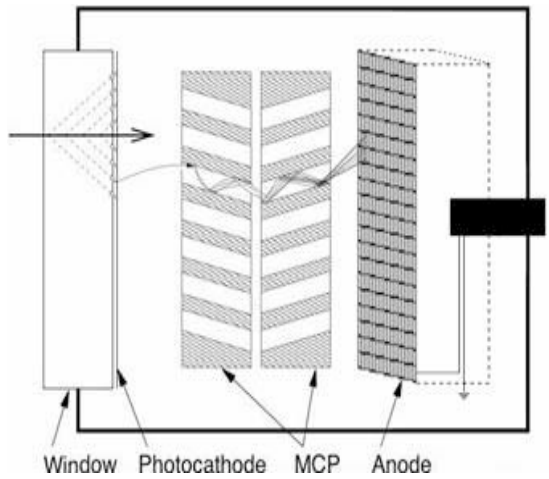

Figure 1: Chevron type MCP.

Problem 1

The potential distribution and electric field for a straight cylindrical pore in a uniform external field (Figure 1) are given by formulae

$$\varphi(\rho,\theta)=\begin{cases}-\dfrac{2\varepsilon_1}{\varepsilon_1+\varepsilon_2}E\rho\cos\theta, & \rho<R,\\ -Ex-E\dfrac{\varepsilon_1+\varepsilon_2}{\varepsilon_1+\varepsilon_2}\dfrac{R^2}{\rho}\cos\theta, & \rho>R.\end{cases} \quad (1)$$

$$E(\rho,\theta)=\begin{cases}\dfrac{2\varepsilon_1}{\varepsilon_1+\varepsilon_2}E\cos\theta, & \rho<R,\\ E-E\dfrac{\varepsilon_1+\varepsilon_2}{\varepsilon_1+\varepsilon_2}\dfrac{R^2}{\rho^2}\cos\theta, & \rho>R.\end{cases} \quad (2)$$

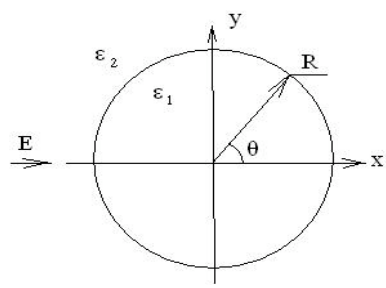

Figure 2: Cylindrical channel of radius R with dielectric constant ε_1 is in the medium ε_2 in an external electric field of strength E.

*Work supported by DoE grant #2005170.
#ivanov@muonsinc.com

Problem 2

The external field can be expanded into parallel and perpendicular components

$$E_0 = E_{\parallel} + E_{\perp}, E_{\parallel} = E_0 \cos\alpha, E_{\perp} = E_0 \sin\alpha. \quad (3)$$

The parallel component does not make a perturbation, but the perpendicular one excites the field of Problem 1. The actual field in a cylindrical channel is

$$E_{\perp}(\rho,\theta) = \frac{2\varepsilon_1}{\varepsilon_1+\varepsilon_2} E_0 \cos\theta \sin\alpha, \quad E_{\parallel} = E_0 \cos\alpha. \quad (4)$$

Finally, the angle between the cylindrical axis and the vector of the internal electric field is

$$\tan\gamma = \frac{E_{\perp}}{E_{\parallel}} = \frac{2\varepsilon_1}{\varepsilon_1+\varepsilon_2} E_0 \cos\theta \tan\alpha. \quad (5)$$

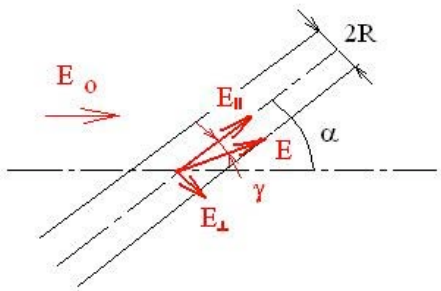

Figure 3: Cylindrical channel in tilted electric field E_0 with angle α.

Problem 3

The presence of conductive material excites surface currents, which increase the electric field from the external side of the layer and decrease it from the internal one – the analogue of a dipole charge layer. It creates the screening effect of lowering for the external field E_{ext} in the pore. The field relaxation ratio for an infinitely thin layer with conductivity σ is

$$k(\sigma) = \frac{E_{\text{int}}}{E_{ext}} = \frac{\sigma_0}{\sigma}, \quad \sigma_0 = \frac{1}{Z_0} = \sqrt{\frac{\varepsilon_0}{\mu_0}} = \frac{1}{376.73\Omega}. \quad (6)$$

An example of fringe-field numerical simulation is presented in Figure 5. Some simulations of the electric field in a tilted pore were done by E.Gatti [12], but no fringe fields were studied there.

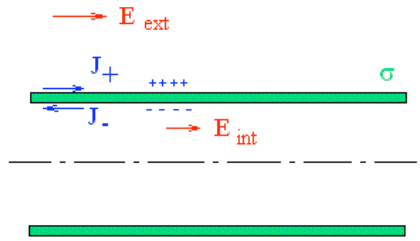

Figure 4: Screening effect of a resistive layer.

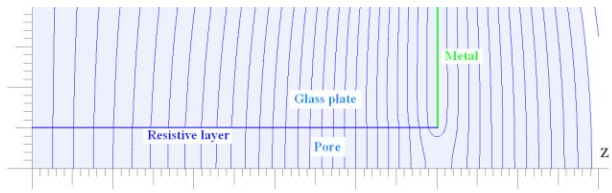

Figure 5: Field map for the fringe field.

DIFFERENT MODELS OF SECONDARY EMISSION

Publication [1] describes a complete model of secondary emission (SE). Here, the energy and angular dependence for true SE is presented by Guest's formula

$$X \equiv \frac{V}{V_{\max}}\sqrt{\cos\theta}, \quad \sigma = \sigma_m X^{\beta} \exp\left[\alpha(1-\cos\theta)+\beta(1-X)\right] \quad (7)$$

where θ – incident angle, V – impact energy, V_{max} – impact energy corresponding to a maximum SE yield of σ_m, α – surface absorption factor, β – smoothness factor (β= 0.55 for $V<V_{max}$, and β=0.25 for $V>V_{max}$). Numerical results of the gain evaluation for MCP thickness L=0.5mm, voltage V = 2kV, σ_m = 3 using Guest's model are shown in Figure 6.

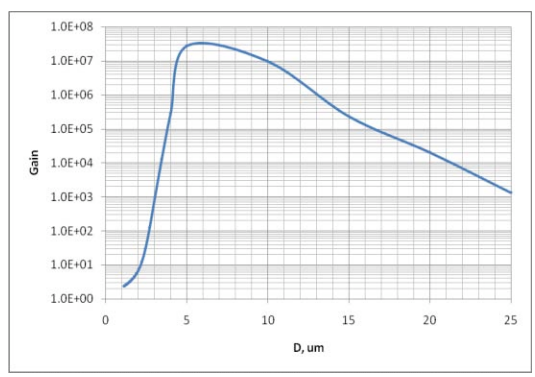

Figure 6: Gain factor vs. MCP diameter D.

The method of MCP simulation [2] was used in modelling of "Planacon" light amplifier (Figure 7) by Burle/Photonics [13]. Our results for simulation (Figures 8-10) show good agreement with experimental data [3], [6]-[7].

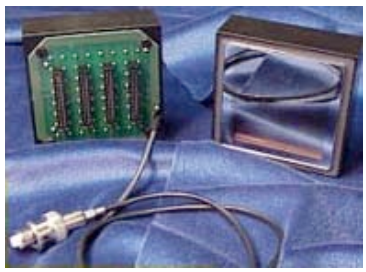

Figure 7. Chevron-type photo multiplier 85022. The MCP is 2"x2" large, there are 1024 anodes, all equally spaced by 1.6 mm. Pore diameter D=25 um.

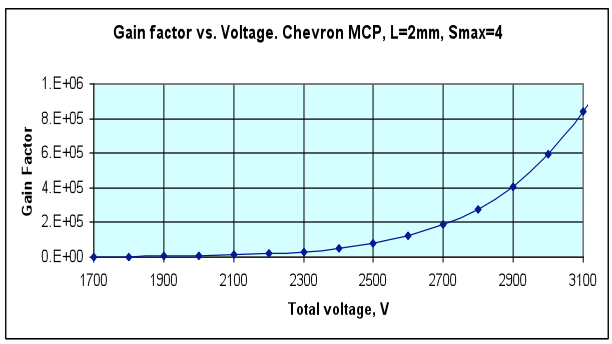

Figure 8. Gain factor vs. MCP voltage.

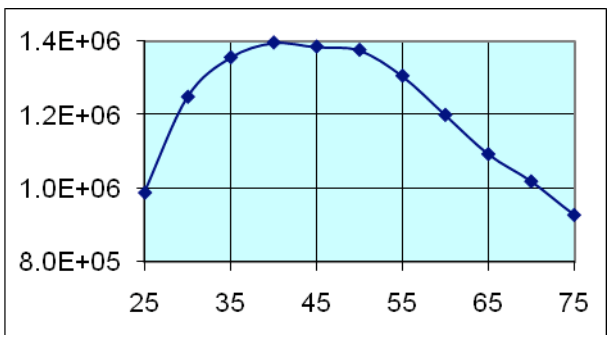

Figure 9. Gain factor vs. ratio L/D. L – length of pore, D – its diameter.

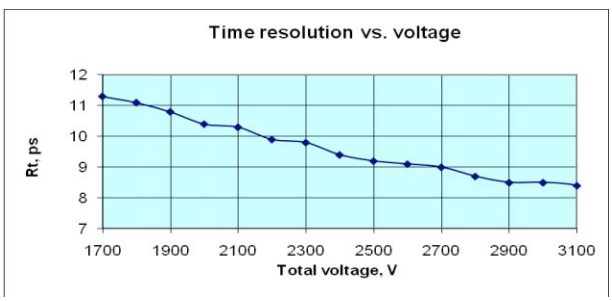

Figure 10. Time resolution including photo cathode – MCP gap,

There are number of other SE models [8-11]. All of them more or less agree each with other for different materials (Figure 11).

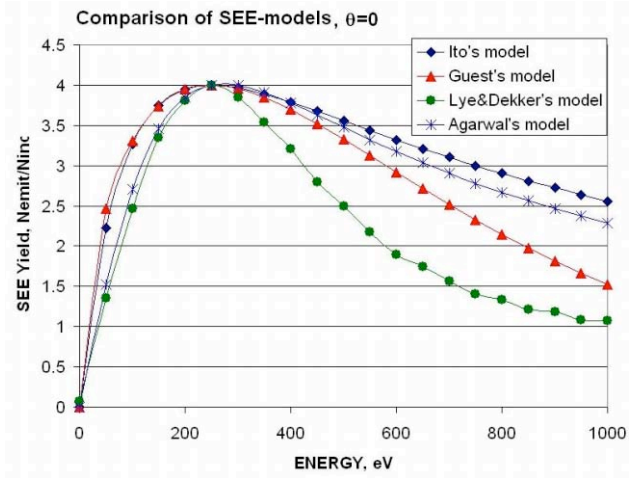

Figure 11: Different models of SE (Courtesy of Z.Insepov).

As for composite materials, these analytical models (Figure 12) do not give good agreement with experimental data.

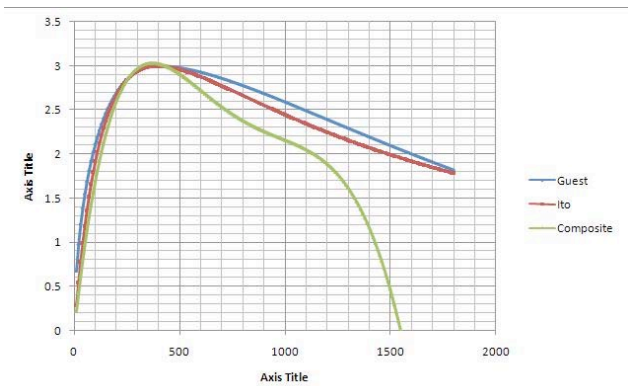

Figure 12: SE curves for a composition of 30% Al_2O_3 + 70% ZnO. Blue – Guest's model; magenta – Ito's models, green – experimental data.

These approximations were used in simulation of the INCOM MCP with parameters: D = 40um, L/D = 40, L = 1.6 mm, voltage U=1kV. The results of numerical simulations of gain and time resolution for different SEE models are presented in Table 1.

Table 1: Comparative analysis of SEE models

Model	Guest	Ito	Composite
Gain	1179	1132	1016
T res., ps	28.3	32.9	26.7

FUNNEL-TYPE MCP SIMULATION

There are ideas for improving the open-area ratio for better determination of the location the first strike, including making the entrance to the channel into a funnel, so that the electron strikes the surface of the

funnel and secondary electrons are sucked into the channel. Alternatively, the funnel could be directly coated with the photo-cathode material, with the photo-electron or electrons then initiating the shower in the channel, as shown in the simulation in Figure 13. The funnel solution is attractive in that it hides the photo-cathode from ion feedback- ions that are created on the channel walls and accelerated back up the channel. These ions are a cause of aging of MCP's, and can be a problem at high gain. Figure 14 demonstrates the result of optimization for photo electron capturing in varying the funnel diameter and photo cathode resistance. The general-purpose electromagnetic and electron optic code "POISSON-2" [14] was used to simulate the two dimensional electrostatic fields and particle tracking.

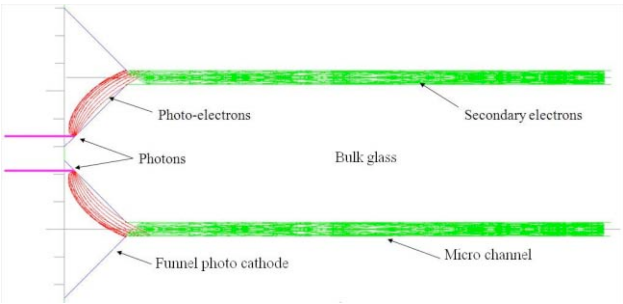

Figure 13: A two of funnel-type cells. Magenta – incoming photon bunches; red – photo electrons; green – cascades of secondary electrons.

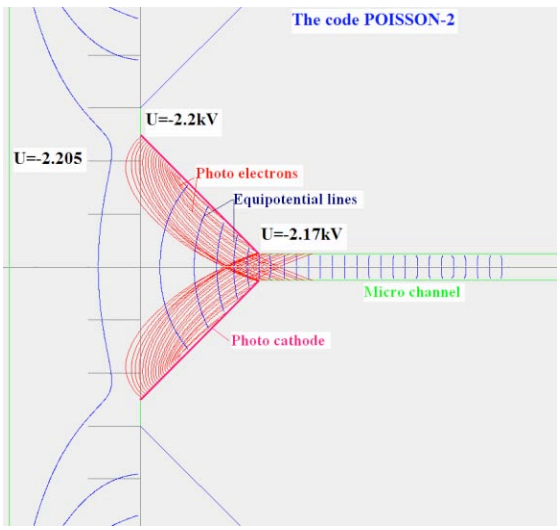

Figure 14: Geometric parameters of the funnel and photo cathode resistance were varied to optimize the capture ratio for photoelectrons.

REFERENCES

[1] A.J. Guest, ACTA Electronica, V.14, N1, 1971, pp. 73-97.
[2] Y.V.Kulikov, Radiotechnika i Svetotechnika, **4**, 1967, pp..376-380.
[3] V.Ivanov, T.Roberts, R.Abrams, H.Frish, PAC'09, 4-8 May, Vancouver, Canada.
[4] V. Ivanov, Micro Channel Plate Simulator, User's Guide, Muons, Inc., 2009.
[5] V. Ivanov. 20-21 July, 2009, Chicago, 1st Workshop on Photo-cathodes: 300nm-500nm.
[6] V. Ivanov, Z.Insepov, Pico-Second Workshop VII, February 26-28, 2009; Argonne National Lab.
[7] V.Ivanov, H.Frish, T.Roberts et al., 27-29 May, 2009, Moscow, IX Seminar on Theoretical & Applied Electron & Ion Optics.
[8] M.Ito, H.Kume, K.Oba, IEEE Trans. on Nucl. Sci., NS-31 , No 1, (1984), pp.408-412.
[9] B.K.Agarwal, Proc. Phys. Soc. (1958), pp.851-852.
[10] E.H.Eberhardt, Appl. Optics, **18**, 9 (1979), pp. 1418-1423.
[11] R.G. Lie, A.J.Dekker, Phys. Rev., Vol.107, N4, 1957.-pp.977-981.
[12] E.Gatti, K.Oha, P.Rehak, IEEE Trans. On Nucl. Sci., NS-30, No 1, (1983), pp.461-468.
[13] http://www.burle.com/prod_showcase.htm.
[14] V. Ivanov. Proc. 2nd Int. Conf. on Computations in Electromagnetism, Nottingham, May 13-15, 1994.